New Journal of Physics
An Institute of Physics and Deutsche Physikalische Gesellschaft Journal

Characterizing carbon nanotube samples with resonance Raman scattering

A Jorio[1,6], M A Pimenta[1], A G Souza Filho[2], R Saito[3], G Dresselhaus[4] and M S Dresselhaus[5]

[1] Departamento de Física, Universidade Federal de Minas Gerais, Belo Horizonte, MG, 30123-970, Brazil
[2] Departamento de Física, Universidade Federal do Ceará, Fortaleza, CE, 60455-760, Brazil
[3] Department of Physics, Tohoku University and CREST JST, Aoba Sendai, 980-8578, Japan
[4] Francis Bitter Magnet Laboratory, Massachusetts Institute of Technology, Cambridge, MA 02139-4307, USA
[5] Department of Physics and Department of Electrical Engineering and Computer Science, Massachusetts Institute of Technology, Cambridge, MA 02139-4307, USA
E-mail: adojorio@cedro.fisica.ufmg.br and adojorio@mgm.mit.edu

New Journal of Physics **5** (2003) 139.1–139.17 (http://www.njp.org/)
Received 15 July 2003
Published 16 October 2003

Abstract. The basic concepts and characteristics of Raman spectra from carbon nanotubes (both isolated and bundled) are presented. The general characteristics of the radial breathing mode, tangential mode (G band), disorder-induced mode (D-band) and other Raman features are presented, with the focus directed toward their use for carbon nanotube characterization. Polarization analysis, surface enhanced Raman spectroscopy and complementary optical techniques are also discussed in terms of their advantages and limitations.

[6] Author to whom any correspondence should be addressed.

1367-2630/03/000139+17$30.00

Contents

1. Introduction

This review is aimed at researchers and engineers who are not experts in Raman spectroscopy, but want to use this technique as an easy and quick characterization tool for carbon nanotube samples. The Raman spectra from carbon nanotubes are rich in information about the structure and properties of nanotubes and the present review should provide a guide for people wanting to understand questions such as: What is the radial breathing mode (RBM) feature in the Raman spectra telling me about my sample? What information is provided by the tangential modes? Should I worry about the laser frequency I am using? Can I use the disorder-induced D band to characterize defects in my sample? Is light polarization important? What can I learn using surface enhanced Raman spectroscopy (SERS) and another optical techniques?

This paper is divided into sections, the first discussing some important experimental details, and the following sections answering each of the questions outlined in the previous paragraph.

2. Some important experimental details

In this paper we discuss the Raman spectra from both isolated and bundled carbon nanotubes. Different carbon nanotube bundled samples were synthesized by different methods, including the chemical vapour deposition (CVD), HiPCo and electric arc methods [1]. Isolated single wall carbon nanotubes (SWNTs) were grown on a Si/SiO_2 substrate containing catalytic iron nano-particles [2], using a CVD method (diameters ranging from about 1 to 3 nm, according to atomic force microscopy (AFM) characterization) [3]. The density of SWNTs μm^{-2} can be controlled during the growth process, basically by controlling the time of growth. Sonication of SWNT bundle samples in solution can also form isolated SWNTs, but the sonication method is less appropriate for single nanotube spectroscopy studies, since introduction of nanotube defects and nanotube fracturing occurs through the sonication process itself, and small bundles often persist after sonication. Nanotubes enclosed by SDS surfactant guarantee that tubes separated

by sonication do not rejoin [4]. However, the presence of the SDS micelles should modify the basic properties of the nanotubes to some extent.

Resonance Raman spectra from SWNTs were acquired using standard commercial micro-Raman spectrometers and lasers, including systems connected with central user facilities, such as a Renishaw (1000B) spectrometer and a Kaiser (Hololab 5000R) single-monochromator micro-Raman spectrometer, and also a Dilor XY triple-monochromator micro-Raman spectrometer, using a back-scattering configuration for all measurements and 50×, 80× and 100× objective lenses (∼1 μm spot size for the 100× objective). Relatively high laser powers (up to 40×10^9 W m^{-2}) can be used to probe isolated SWNTs because of their unusually high thermal conductivity values (3000 W m^{-1} K^{-1}) [5], their excellent high temperature stability and their good thermal contact to the substrate. A triple-monochromator is ideal for the Raman measurements while tuning the excitation laser line continuously, but the acquired intensity drops substantially when compared to the intensity obtainable from a single-monochromator spectrometer. We have measured the Raman spectra from SWNTs using discrete lines from Ar–Kr and He–Ne lasers and also using a continuous range of excitation energies from both a Ti:sapphire and a dye laser. We have observed stable nanotube Raman signals for laser powers impinging on the substrate up to 40 mW into a 100× objective. We usually use laser powers of about 10 mW in our measurements, although measurements have been carried out successfully with laser power levels down to 1 mW ($\sim 1 \times 10^9$ W m^{-2}).

In the process of measuring the Raman spectra from isolated SWNTs on a Si/SiO_2 substrate using a fixed laser energy E_{laser}, we focus the laser spot on the substrate surface and we scan the sample until we observe the Raman signal from an isolated SWNT. The Raman intensity from SWNTs is usually buried under the noise, except for a few (n, m) SWNTs for which the resonance with the given E_{laser} occurs strongly for the electronic states confined within the van Hove singularities (vHSs). The observation of the weak Si feature at 303 cm^{-1} is a useful guide for knowing whether the radial breathing Raman mode from an isolated SWNT can be measured. Figure 1(a) shows an example of Raman signals from two resonant SWNTs in two different spots on the Si/SiO_2 surface. The peaks at 156 and 192 cm^{-1} are the RBMs from the resonant SWNTs, while the step at 225 cm^{-1} and the peak at 303 cm^{-1} come from the Si substrate. For various experiments of interest, we have used samples with a variety of nanotube densities, ranging from low density samples (∼0.4 SWNT μm^{-2}) to higher density samples (∼10 SWNT μm^{-2}). Samples with a high nanotube density (more than 1 SWNT μm^{-2}) guarantee that the search for resonant nanotubes will not be so tedious, but a low density sample (less than 1 SWNT μm^{-2}) guarantees that one will not get a Raman signal from two or more SWNTs within the same light spot. A spectrum containing a signal from more than one SWNT restricts the wealth of information that is provided at the single nanotube level.

Figure 1(b) gives a general view of the Raman spectra from a sample of SWNT bundles. The lower trace shows the two dominant Raman features, the RBM and the tangential (G band) features. In the upper trace, the background intensity is increased to show the rich Raman spectra over the entire first- and second-order phonon frequency range between the RBM and G features, including the disorder-induced D band and other lower intensity features. The power used to measure the Raman spectra for SWNT bundles without burning the sample should be much lower than for isolated SWNTs, usually not higher than 1 mW using a 100× objective lens.

The Raman features are analysed by a Lorentzian fit of the spectra, with the exception of the lower frequency G-band feature, denoted by G^-, which, for metallic SWNTs is observed to have a Breit–Wigner–Fano (BWF) lineshape (broad and asymmetric peak), though the G^-

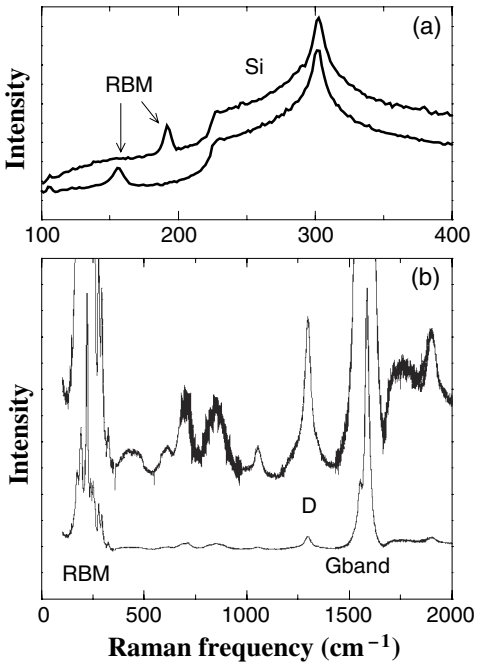

Figure 1. (a) Typical Raman spectra from a Si/SiO_2 substrate at the SWNT RBM frequency region, taken from two different spots where the Raman signal from isolated resonant SWNTs are observed. The peaks at 156 and 192 cm^{-1} are the RBM from resonant SWNTs, while the steps at 225 cm^{-1} and the peaks at 303 cm^{-1} come from the substrate. The spectra were taken with a single monochromator, six accumulations of 30 s, 10 mW of the 514 nm laser ($E_{laser} = 2.41$ eV) impinging on the sample through a 50× objective. (b) Raman spectra from SWNT bundles taken with $E_{laser} = 2.41$ eV. The most intense features are the RBM and G-band. The background is enlarged to show the richness of the Raman spectra from SWNTs over this large frequency range.

feature for semiconducting SWNTs remains Lorentzian. Although it is known that the disorder-induced D band appears in the Raman spectra of graphite-like materials through a double resonance process [6, 7], where inhomogeneous broadening occurs, we use the Lorentzian fit as an approximation to interpret the behaviour of the D band.

3. Importance of the electronic structure and excitation laser energy

Usually Raman spectra only involve phonons explicitly, being independent of the electronic structure of the material and the laser energy used to excite the Raman spectra. Furthermore, the usual Raman scattering signal is weak. However, the scattering efficiency gets larger when the laser energy matches the energy between optically allowed electronic transitions in the material, and this intensity enhancement process is called resonance Raman scattering [8]. The resonance Raman intensity depends on the density of electronic states (DOS) available for the optical transitions, and this property is very important for one-dimensional (1D) systems, as we discuss in what follows.

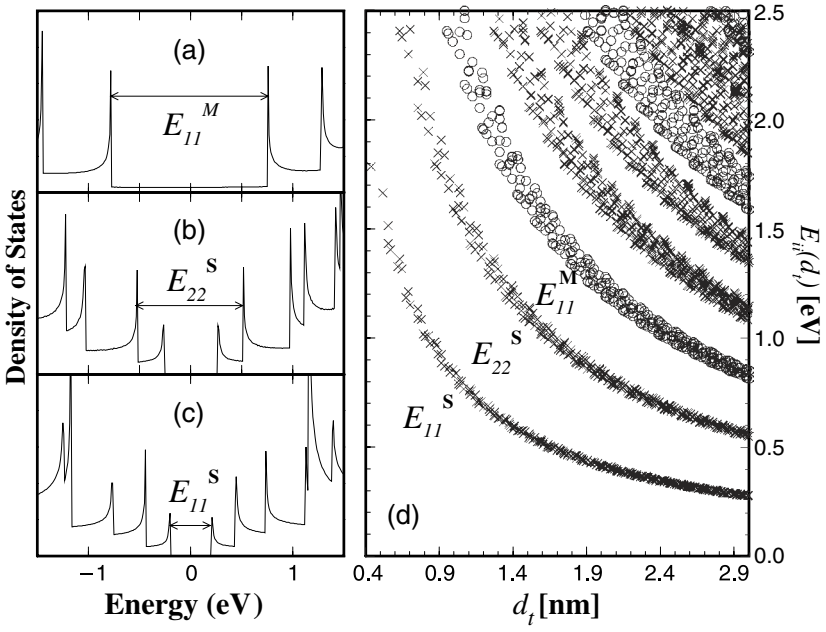

Figure 2. DOS for a (a) armchair (10, 10) SWNT, (b) chiral (11, 9) SWNT and (c) zigzag (22, 0) SWNT obtained with the tight binding model from [13]. (d) Shows the electronic transition energies E_{ii} for all the (n, m) SWNTs with diameters from 0.4 and 3.0 nm using a simple first-neighbour tight binding model [14]. Distortion from this simple one-electron model is expected for the lower energy transitions E_{11}^{S} and for SWNTs with $d_t < 1$ nm.

Figures 2(a)–(c) shows the DOS for three different SWNTs, and since SWNTs are 1D systems, their DOS is characterized by the so-called van Hove singularities (vHSs). The sharp vHSs define narrow energy ranges where the DOS intensity becomes very large. Therefore, in practice, a single carbon nanotube exhibits a 'molecular-like' behaviour, with well defined electronic energy levels at each vHS. The three DOS curves in figures 2(a)–(c) come from different SWNTs as labelled by their (n, m) indices [9] (see caption). Each pair of indices defines a unique way to roll up the graphene sheet to form the nanotube, and each unique (n, m) nanotube has a distinct electron and phonon structure. An observable Raman signal from a carbon nanotube can be obtained when the laser excitation energy is equal to the energy separation between vHSs in the valence and conduction bands (e.g., see E_{11}^{S}, E_{22}^{S} and E_{11}^{M} in figure 2), but restricted to the selection rules for optically allowed electronic transitions [10]–[12]. Because of this resonance process, Raman spectra at the single nanotube level allow us to study the electronic and phonon structure of SWNTs in great detail. When Raman spectra of SWNT bundle samples are taken, only those SWNTs with E_{ii} in resonance with the laser excitation energy E_{laser} will contribute strongly to the spectrum.

For the characterization of nanotubes by Raman spectroscopy, it is useful to consider plots of the energies E_{ii} versus the nanotube diameter, d_t, as shown in figure 2(d) [15]. Each point in this plot represents one optically allowed electronic transition energy (E_{ii}) from a given (n, m) SWNT. Crosses come from semiconducting SWNTs, and circles from metallic SWNTs. This plot should be considered as a guide for answering the question 'if I use a given E_{laser} to excite

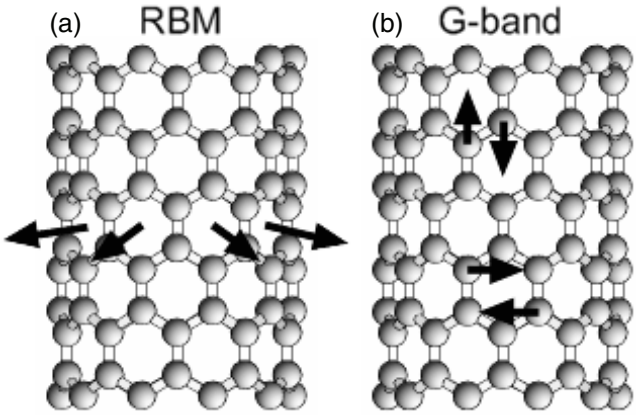

Figure 3. Schematic picture showing the atomic vibrations for (a) the RBM and (b) the G band modes.

my sample, which (n, m) carbon nanotubes can be in resonance with my laser line?' In other words, since the observable Raman spectra come predominantly from tubes in resonance with E_{laser}, figure 2 specifies the nanotubes that will be observable for a given laser line.

4. Radial breathing modes—RBM

The RBM Raman features (appearing between 120 $\text{cm}^{-1} < \omega_{\text{RBM}} < 250\ \text{cm}^{-1}$ for SWNTs within 1 nm $< d_t <$ 2 nm) correspond to the atomic vibration of the C atoms in the radial direction, as if the tube was breathing (see figure 3). These features are very useful for characterizing nanotube diameters through the relation $\omega_{\text{RBM}} = A/d_t + B$, where the A and B parameters are determined experimentally. For typical SWNT bundles in the diameter range $d_t = 1.5 \pm 0.2$ nm, $A = 234\ \text{cm}^{-1}$ nm and $B = 10\ \text{cm}^{-1}$ has been found for SWNT bundles [16] (where B is an upshift coming from tube–tube interaction). For isolated SWNTs on an oxidized Si substrate, $A = 248\ \text{cm}^{-1}$ nm and $B = 0$ have been found [3, 17]. It is important to point out that, for the usual diameter range 1 nm $< d_t <$ 2 nm, these two sets of parameters give similar d_t for a given ω_{RBM}, differing considerably only for $d_t <$ 1 nm and $d_t >$ 2 nm (see figure 4). However, for $d_t <$ 1 nm, the simple $\omega_{\text{RBM}} = A/d_t + B$ relation is not expected to hold due to nanotube lattice distortions leading to a chirality dependence of ω_{RBM} [18]. For large diameter tubes ($d_t >$ 2 nm) the intensity of the RBM feature is weak and is hardly observable.

As discussed in the previous section, it is useful to have the (E_{ii} versus d_t) plot (figure 2(d)) on hand when acquiring the RBM spectra from a SWNT sample. Figure 5 shows a connection between the (E_{ii} versus $1/d_t$) plot (bottom) and the (I_{RBM} versus ω_{RBM}) Raman spectra (top) using the relation $\omega_{\text{RBM}} = 248/d_t$. Suppose that one measures the Raman spectra from a sample composed of all the possible (n, m) nanotubes (real samples usually exhibit a Gaussian diameter distribution around some mean diameter, but this contrived sample will be used here for gaining an understanding of how to use figure 2(d)). The hypothetical Raman spectra that would be observed from this sample would depend on the energy of the excitation laser light, and using $E_{\text{laser}} =$ 1.58 eV (785 nm from the Ti:sapphire laser) for example, the Raman spectra would look like the curve shown in figure 5(a). This Stokes spectra was calculated considering the Raman cross section to be proportional to the square of $1/[(E_{\text{laser}} - E_{ii} + \text{i}\Gamma_r)(E_{\text{laser}} - E_{ii} - E_{\text{phonon}} + \text{i}\Gamma_r)]$,

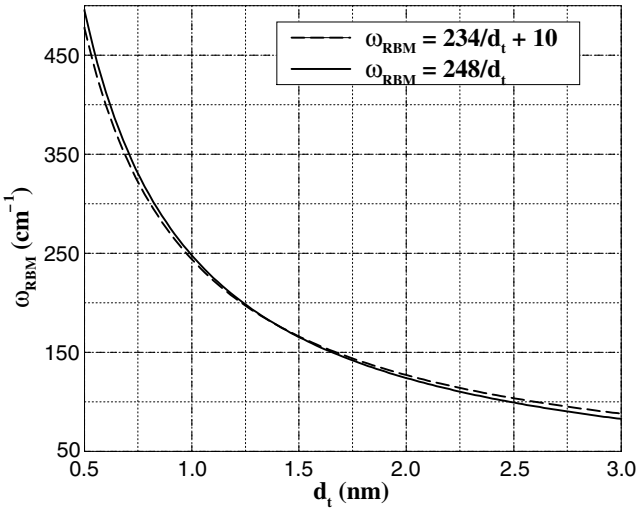

Figure 4. RBM frequencies $\omega_{\mathrm{RBM}} = A/d_{\mathrm{t}} + B$ versus nanotube diameter for: (i) $A = 234\ \mathrm{cm}^{-1}$ nm and $B = 10\ \mathrm{cm}^{-1}$, for SWNT bundles [16] (dashed curve); (ii) $A = 248\ \mathrm{cm}^{-1}$ nm and $B = 0$, for isolated SWNTs [3, 17] (solid curve).

to account for the resonance Raman process [16]. E_{phonon} is the phonon energy and Γ_r is the broadening factor related to the lifetime for the excited state ($\Gamma_r = 8$ meV [20]). For the Raman spectra of a real sample taken with a given E_{laser}, the resonance profile will be compounded by the Gaussian distribution of the sample.

It is clear that a single Raman measurement gives an idea of the tubes that are in resonance with that laser line, but does not give a complete characterization of the diameter distribution of the sample. However, by taking Raman spectra using many laser lines, a good characterization of the diameter distribution in the sample can be obtained [16].

The natural linewidths for the RBM feature observed for isolated SWNTs are $\gamma_{\mathrm{RBM}} = 3\ \mathrm{cm}^{-1}$, although larger Γ_{RBM} values are usually observed due to broadening effects [19]. The broadening has been observed to increase as the SWNT diameter is increased, and $\Gamma_{\mathrm{RBM}} > 20\ \mathrm{cm}^{-1}$ values have been observed for $d_{\mathrm{t}} > 2$ nm [19]. For the features observed in SWNT bundles, the linewidth will not reflect Γ_{RBM}, but it will rather reflect the ensemble of tubes in resonance with E_{laser}.

In summary, a careful analysis of figure 2(d), considering the E_{laser} line to be used, should be made to correctly understand the RBM information that can be obtained from the Raman spectra from an actual SWNT sample.

It is also important to point out that, at the single isolated SWNT level, accurate determination of the E_{ii} for the resonant SWNT can be done by using a tunable laser (E_{ii} definition with $\pm 3\ \mathrm{cm}^{-1}$ accuracy—see [20]), or simply by measuring the Stokes and anti-Stokes signals, E_{ii} can be obtained with a single laser line (E_{ii} definition with $\pm 10\ \mathrm{cm}^{-1}$ accuracy—see [21]).

5. Tangential modes—G band

The observation of characteristic multi-peak features around $1580\ \mathrm{cm}^{-1}$ also provides a signature of carbon nanotubes. Spectra in this frequency range can be used for SWNT characterization, independent of the RBM observation. This multi-peak feature can, for example, also be used for diameter characterization, although the information provided is less accurate than the RBM

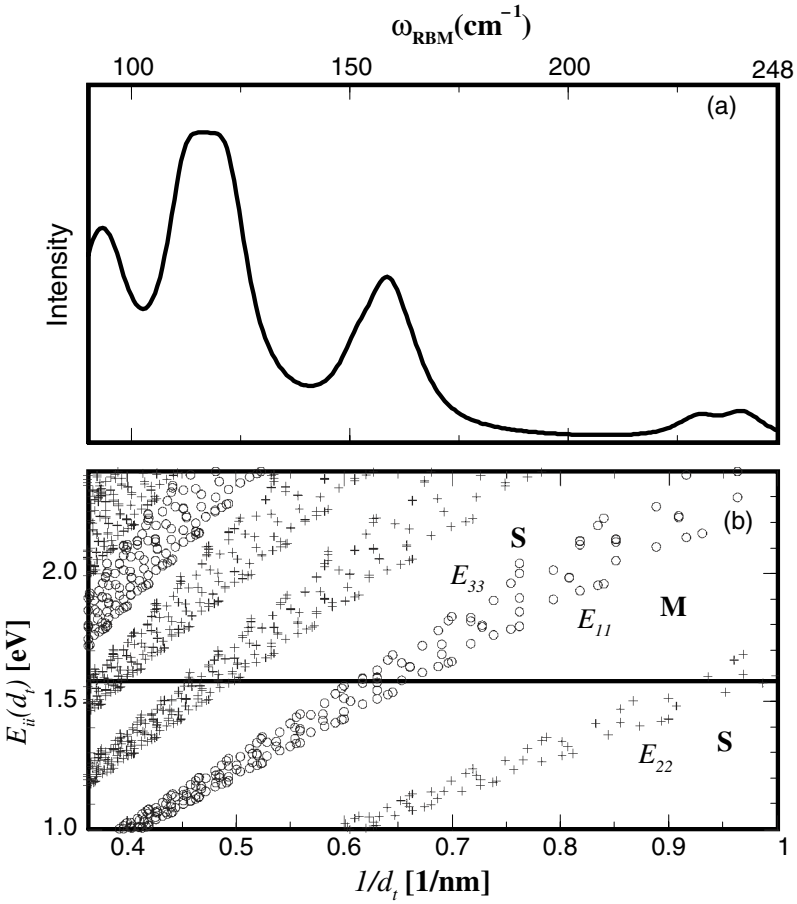

Figure 5. (a) RBM Raman intensity I_{RBM} versus RBM frequency ω_{RBM} for an hypothetical sample composed of all the possible (n, m) SWNTs, excited with $E_{\mathrm{laser}} = 1.58$ eV. Lorentzian linewidths $\gamma_{\mathrm{RBM}} = 3\ \mathrm{cm}^{-1}$ were used [19]. For calculation details, see [16]. (b) E_{ii} versus $1/d_{\mathrm{t}}$ plot. The x-axis for the two plots are connected by the relation $\omega_{\mathrm{RBM}} = 248/d_{\mathrm{t}}$. The horizontal line in (b) shows the E_{ii} transitions for the SWNTs in resonance with $E_{\mathrm{laser}} = 1.58$ eV.

feature, and it gives information about the metallic character of the SWNTs in resonance with a given laser line.

The Raman-allowed tangential mode in graphite is observed at 1582 cm^{-1}, and is called the G mode (from graphite) (see figure 6). Unlike graphite, the tangential G mode in SWNTs gives rise to a multi-peak feature, also named the G band, where up to six Raman peaks can be observed in a first-order Raman process. However, a simple analysis can be carried out considering the two most intense peaks, that basically originate from the symmetry breaking of the tangential vibration when the graphene sheet is rolled to make a cylindrically shaped tube (see figure 3). The two most intense G peaks are labelled G^{+}, for atomic displacements along the tube axis, and G^{-}, for modes with atomic displacement along the circumferential direction (see figures 3 and 6), and the lowering of the frequency for the G^{-} mode is caused by the curvature of the nanotube which softens the tangential vibration in the circumferential direction.

The difference between the G band lineshape for semiconducting and metallic SWNTs is evident in the lineshape of the G^{-} feature (see figure 6), which is broadened for metallic SWNTs

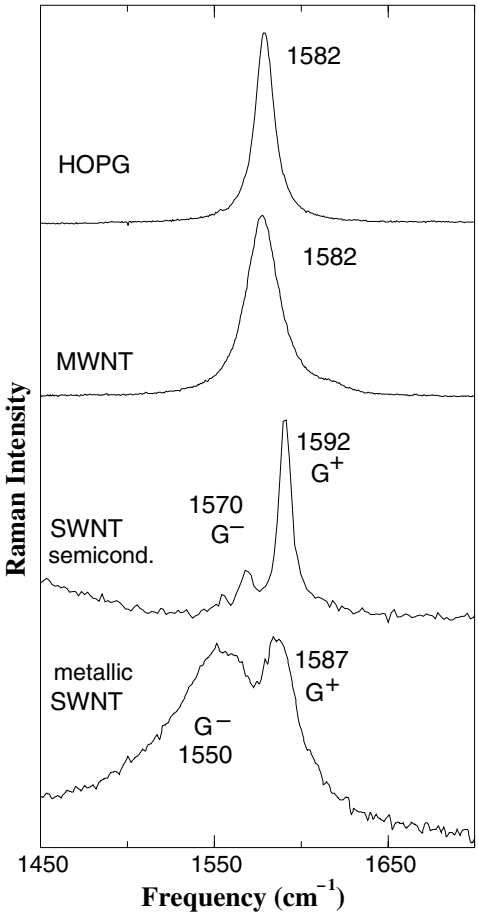

Figure 6. G band for highly ordered pyrolytic graphite (HOPG), MWNT bundles, one isolated semiconducting SWNT and one isolated metallic SWNT. The multi-peak G-band feature is not clear for MWNTs due to the large tube diameters (see section 10).

in comparison with the Lorentzian lineshape for semiconducting tubes, and this broadening is related to the presence of free electrons in nanotubes with metallic character [22, 23]. This broadened G^- feature is usually fit using a BWF line that accounts for the coupling of a discrete phonon with a continuum related to conduction electrons [23, 24]. This BWF line is observed in many graphite-like materials with metallic character, such as n-doped graphite intercalation compounds (GIC) [25], n-doped fullerenes, as well as metallic SWNTs.

Considering the (E_{ii} versus d_t) plot in figure 2(d), for a given E_{laser} line, one can predict the diameter range where semiconducting-like G^- band lineshapes will be observed and the diameter range for which the metallic-like G^- band should be observed [22]. Observation of a metallic-like G band when a semiconducting lineshape should be observed indicates the presence of charged impurities [26].

Figure 7 shows the diameter dependence of the G^+ frequency (ω_{G^+}) and the G^- frequency (ω_{G^-}) for metallic and semiconducting SWNTs (see also figure 9). While ω_{G^+} is practically independent of tube diameter, ω_{G^-} decreases when decreasing d_t, and this decrease becomes larger as the curvature of the sheet increases [27, 28]. Therefore, the splitting $\Delta\omega_G = \omega_{G^+} - \omega_{G^-}$ can be used for diameter characterization (see table 1). If isolated SWNTs are measured, the

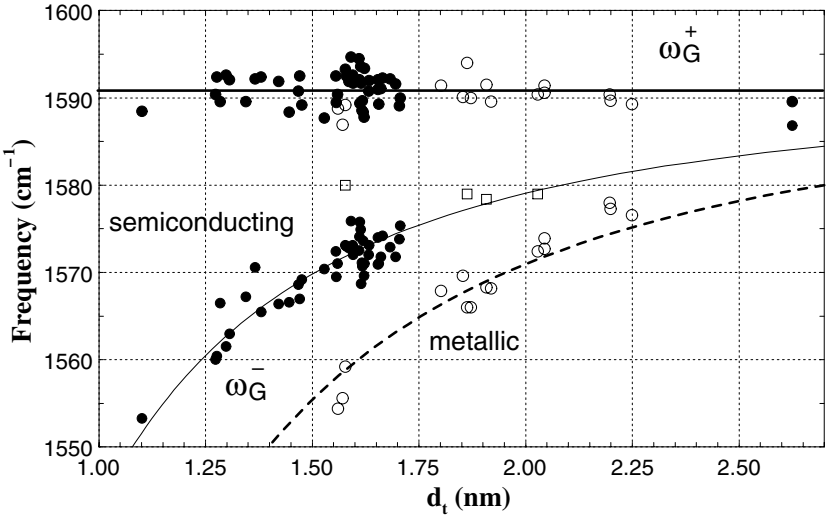

Figure 7. Diameter dependence for ω_{G^+} and ω_{G^-} for several isolated semiconducting and metallic SWNTs. Filled and open symbols apply for semiconducting and metallic tubes, respectively. The lines are fit to the experimental points (see table 1).

value of $\Delta\omega_G$ refers to the particular tube in question, but if SWNT bundles are measured, the $\Delta\omega_G$ will be roughly related to the maximum in the Gaussian diameter distribution of the sample, but does not accurately reflect the diameter dependence of ω_{G^-} [29].

The linewidths Γ_{G^+} for the G peaks from isolated SWNTs are usually around 5–15 cm^{-1}, and the same range of linewidths for Γ_{G^-} are found for semiconducting isolated SWNTs [19]. For semiconducting SWNTs in bundles, the linewidths are related to the diameter distribution, and therefore the broadening principally occurs for Γ_{G^-}. For metallic SWNTs, the broadening is minor for Γ_{G^+}, while for Γ_{G^-} a significant broadening occurs, and it is found that the linewidth for the BWF line is strongly dependent on tube diameter. For isolated tubes with $d_t > 2$ nm, Γ_{G^-} is similar to semiconducting SWNTs, and the line mostly looks like a normal Lorentzian, reflecting the small magnitude of the BWF effect. The BWF effect increases as the tube diameter decreases, causing the G^- feature to become more asymmetric and broad (see figure 9). Values of $\Gamma_{G^-} > 70$ cm^{-1} have been observed for isolated metallic SWNTs [19].

It is important to comment here that there are recent works reporting evidence for the G band Raman signal originating from a double resonance mechanism [30, 31]. In such a case, the G band intensity depends on defects and its frequency is E_{laser} dependent, making it complicated to use their Raman spectra for SWNT characterization. However, it can be shown that the double resonance and single resonance mechanisms exhibit the same intensity in a defective material, while the single resonance process is two orders of magnitude higher in intensity than the double resonance process for a good quality aligned sample [32], and the Raman spectra can be used for SWNT characterization of good quality samples.

6. Polarization analysis

Polarization of the incident and scattered light is not an important issue for a sample of misaligned carbon nanotubes, but polarization effects are very important for the Raman response of a sample of aligned carbon nanotubes (either aligned bundles or a single straight carbon nanotube).

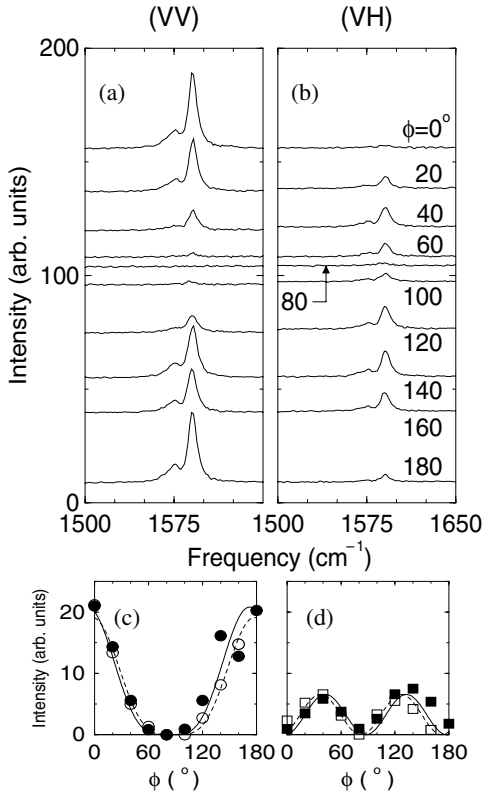

Figure 8. Polarization dependence of the G band from one isolated semiconducting SWNT sitting on a Si/SiO_2 substrate [39] with incident and scattered light parallel (a) and crossed (b) to each other. $\phi = 0°$ stands for incident light polarized along the nanotube axis. Points on (c) and (d) plot the G-band intensity dependence on ϕ for (a) and (b), respectively. The solid curves fit the data points with the fuctions $\cos^4(\phi)$ and $\cos^2(\phi)\sin^2(\phi)$.

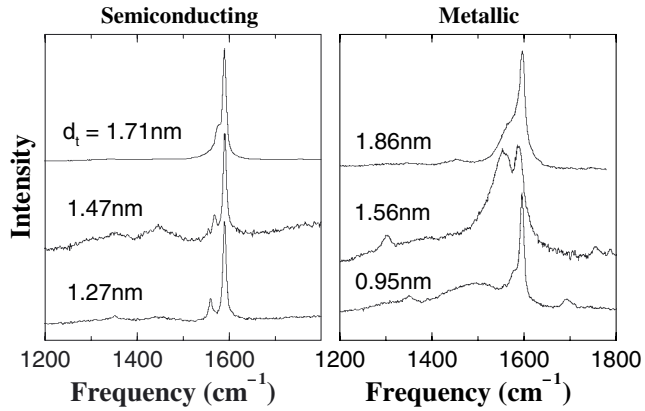

Figure 9. Raman signal from three isolated semiconducting and three isolated metallic SWNTs showing the G and D band profiles. SWNTs in good resonance (strong signal with low signal to noise ratio) show practically no D band. Spectra in bad resonance shows noisy background with a peak at $\sim$1450 cm^{-1} (e.g., see second trace for semiconducting SWNTs).

Table 1. Diameter dependence of some features observed in the Raman spectra of isolated SWNTs. Here ω_0 denotes the mode frequency associated with 2D graphite, whose value depends on the laser excitation energy, if the mode is associated with a double resonance process. Frequencies are in units of cm^{-1} and d_t is in units of nm. The coefficients for the D, M and G′ bands were obtained by using data measured with $E_{laser} = 2.41$ eV.

$\bar{\omega} = \omega_0 + \beta/\bar{d}_t^n$			
Mode	Frequency ω_0	Exponent n	Diameter coefficient β
RBM	0	1	248[a]
D	ω_D^0	1	−16.5[b]
G^+	1591	0	0
G^-	1591	2[c]	(−45.7; −79.5)[d]
M^+	$\omega_{M^+}^0$	1	−18.0[e]
M^-	$\omega_{M^-}^0$	1	−16.7[e]
G′	$\omega_{G'}^0$	1	−35.4[b]

[a] Reference [3].
[b] This value was obtained using the $E_{laser} = 2.41$ eV. By using the spectra obtained with 1.58 eV, a −18.9 value for β was obtained for the D band [42].
[c] The coefficient $n = 2$ was found by analysing the G band with only two Lorentzian peaks [27]. A different value is found when using six Raman allowed peaks to fit the G-band spectra [28].
[d] The coefficient β for the G^- component is, respectively, −45.7 and −79.5 cm^{-1} nm^2 for semiconducting and metallic SWNTs, and 1.58, 2.41 and 2.54 eV laser lines were used to obtain the G-band experimental results used in the fitting procedure [27].
[e] Reference [43].

Although strict polarization studies require selection rules and phonon/electron symmetry analysis [28, 33, 34], there is a general and simple polarization behaviour that one should have in mind when acquiring the Raman spectra from a sample of aligned carbon nanotubes. Carbon nanotubes behave as antennas, with the absorption/emission of light being highly suppressed for light polarized perpendicular to the nanotube axis [35, 36]. Therefore, if one wants to measure Raman spectra from a sample of aligned carbon nanotubes, the largest Raman intensity will be generally observed for light polarized along the tube axes, and almost no signal will be observed for cross polarized light (see figure 8) [37]–[40]. This 'antenna effect' is found to become less efficient as the tube diameter increases, but the polarization effect is highly effective in the range $0.4\ \text{nm} < d_t < 2\ \text{nm}$.

In single nanotube spectroscopy, where the sample is not optically visible, it is helpful to optimize the signal by using a $\lambda/2$ wave plate to rotate the polarization of the incident and scattered light [37]. Attention to the polarization of the light is important for carrying out quantitative studies of the Raman intensity.

7. Disorder-induced D band

The first question one has about the D band in the carbon nanotube spectra is: 'Can I use it for defect characterization?' Up to now, there is no definitive answer to this question since no systematic study has yet been carried out to correlate the presence of the D band with different defect types (such as hetero-atoms, vacancies, heptagon–pentagon pairs, kinks, or even the presence of impurities, etc). However, relevant information has been obtained, as discussed in what follows.

From a large number of Raman spectra from isolated SWNTs (over 100 signals from physically different tubes), about 50% exhibit observable D band signals with weak intensity (usually 100 times smaller than the G band—see figure 9). In isolated carbon nanotubes, a large D peak compared with the G peak usually means a bad resonance condition (i.e., E_{laser} is not close to E_{ii}). In these cases, the observation of a peak around 1450 cm^{-1} is also common (see figure 9). Note that in figure 1(b) the D band is very weak, with an intensity similar to the many other SWNT features observed in the frequency range between the RBM and the G band, discussed in the following section. The observation of large D-band peaks compared with the G peak intensity in SWNT bundles usually indicates the presence of amorphous carbon [41].

There are two characteristics that differentiate the D band in carbon nanotubes from the D band in defective graphite.

(1) *Small linewidths.* From the observation of a large number of D band features from isolated SWNTs, Γ_{D} values from 40 cm^{-1} down to 7 cm^{-1} have been observed [19]. It is usual to observe the Raman spectra from SWNT samples to be composed of a broad peak upon which is superimposed a sharper peak, the broad feature coming from amorphous carbon and the sharper feature coming from the carbon nanotubes.

(2) *Lower frequencies.* The D-band frequency ω_{D} in carbon nanotubes is usually lower than ω_{D} from bulk sp^2-based carbons, and the downshift increases with decreasing tube diameter, with ω_{D} showing a $1/d_{\text{t}}$ dependence [42]. This frequency dependence on tube diameter is actually not a unique D-band characteristic, but it is observed for other Raman features, as summarized in table 1.

Finally, the D band also exhibits a very important property that is a frequency dependence on chiral angle. This topic will be discussed in the next section together with other chirality-dependent features.

8. Other Raman features

The rich spectral features between the RBM and G modes (see figure 1(b)) originate from either a double-resonance process [6, 7] or from folding the phonon dispersion of 2D graphite into a 1D Brillouin zone. Most of the peaks are so weak that they must be viewed on an expanded scale to appear clearly in the spectra, and the physics needed to understand their behaviour is also more sophisticated.

These peaks are interesting for nanotube characterization, first because they give information about many phonon branches, important for transport, thermal and mechanical properties of carbon nanotubes, and second because they exhibit chirality-dependent frequencies. This chirality dependence of the peak frequencies for the weak spectral features can be understood, considering that they come from the interior of the anisotropic 2D phonon Brillouin zone.

Different (n, m) nanotubes mean different folding of the 2D phonon dispersion. For a fixed phonon wavevector magnitude $|q|$ from a high symmetry point (e.g., the K point), the phonon frequencies are different for different phonon propagation directions. During the folding process, this property results in having the phonon frequencies for nanotubes with fixed diameters, depend on chiral angle. For example, the D band was shown to exhibit a $\Delta\omega_{\mathrm{D}} = 24\ \mathrm{cm}^{-1}$ frequency difference between armchair and zigzag carbon nanotubes [44].

However, this analysis is useful mostly for isolated SWNTs. For SWNT bundles, the D-band spectrum usually shows an overlap of many peaks from different (n, m) tubes in resonance with E_{laser}. Analysis of the detailed lineshape of the D-band can be performed based on resonance Raman theory [45]. Similar chirality-dependent effects are observed for the other weak features in the Raman spectra occurring in the spectral region between the RBM and G-band features.

9. Complementary optical techniques

SERS can be considered as a complementary technique to probe carbon nanotubes. SERS has been developed to probe the Raman spectra from single molecules, whose weak Raman signal would not otherwise be observable. In the case of carbon nanotubes, this technique can be important for observing the Raman spectra from carbon nanotubes that do not satisfy the resonance condition for a given E_{laser}. Although many studies have been carried out to show the enhancement of the Raman signal from carbon nanotubes when using SERS [46]–[49], a systematic study of the difference between SERS enhanced versus resonantly enhanced carbon nanotube signals is still to be performed.

Infrared (IR) spectroscopy, optical absorption and luminescence have also been used to study carbon nanotubes. IR has been applied to SWNT bundles [50, 51], optical absorption has been used to study both isolated SWNTs [4] and carbon nanotube bundles [15], while luminescence has been observed from isolated semiconducting SWNTs [4].

For phonon studies, Raman spectroscopy has been by far the most informative and sensitive technique. The IR signal from carbon nanotubes is very weak [50, 51], and it does not exhibit the rich resonance effect that couples electrons to photons. However, IR has been used to study the plasma frequency in carbon nanotubes and the presence of mini-gaps (meV) in 'quasi-metallic' SWNTs [51]. Furthermore, a quantitative procedure for the evaluation of the carbonaceous purity of bulk quantities of as-prepared SWNT soot can be obtained by the utilization of solution-phase near-IR spectroscopy [52].

For electronic studies, optical absorption and luminescence have strong advantages over Raman spectroscopy:

(i) the signals are usually much stronger;

(ii) scanning over excitation laser energies is usually easier;

(iii) these techniques usually probe lower energy bands, such as E_{11}^{S}, which are not as accessible with standard available Raman equipment.

These techniques can also be used for E_{ii} measurements, although for a complete structural (n, m) assignment, they require additional information that can be obtained only from using joint techniques, such as Raman measurements of the RBMs, for example [4, 53]. Furthermore, the luminescence signal can only be observed for isolated semiconducting SWNTs. Bundled tubes usually exhibit non-radiative electron–phonon recombination processes that greatly restrict the

excited state photon lifetime and strongly compete with the luminescence process [4, 53]. Also metallic tubes have no energy bandgap, and therefore there is no corresponding light emission.

10. Multi-wall carbon nanotubes—MWNTs

For Raman scattering, multi-wall carbon nanotubes can be said to be an ensemble of carbon nanotubes with diameters ranging from small to very large. Because of the large diameter of the outer tubes for typical MWNTs, most of the characteristic differences that distinguish between the Raman spectra in carbon nanotubes from that for graphite are not so evident in MWNTs. The Raman features associated with the small diameter inner tubes can sometimes be observed when a good resonance condition is established [54, 55], but it is not the usual result. The RBM from large diameter tubes is usually too weak to be observable. Figure 6 shows the G band for a MWNT bundle sample. The shoulder at higher frequency ($\sim$1618 cm^{-1}) is typical of defective graphite-like materials and can be smaller in better quality MWNT samples. Whereas the $G^+ - G^-$ splitting is large for small diameter tubes (see section 5), this double-peak G band splitting for large diameter MWNTs is both small and smeared out because of the diameter distribution and therefore the G feature predominantly exhibits a weakly asymmetric characteristic lineshape, with a peak appearing at the graphite frequency 1580 cm^{-1}. These properties makes it more difficult to differentiate the Raman signal of MWNTs from that of graphite.

11. Final remarks

It is important to stress once more that when studying the Raman signal from SWNTs, the Kataura plot of E_{ii} versus d_t, showing the (n, m) SWNTs for which $E_{\text{laser}} = E_{ii}$, should be used as a guide for understanding the Raman spectra from SWNTs, both in bundles and as isolated tubes. A simple tight binding model considering only nearest-neighbour coupling ($\gamma_0 = 2.9$ eV and $s = 0$) is satisfactory for interpreting most of the features of the general Raman spectra. For small diameter tubes (below 1 nm) and for lower energy transitions E_{11}^S a more complete model must be considered [4, 17].

The use of Raman spectroscopy for characterizing SWNT bundles is easy, and is one of the best characterization tools. Even on 'dirty' samples (full of amorphous carbon, catalyst or any other impurities), it is common that high laser powers burn impurities first, leaving cleaner SWNT samples behind [56, 57]. This process can be followed by an improvement in the characteristic Raman signal of the sample when the incident laser power is slowly increased. Raman spectroscopy becomes even more powerful for isolated SWNTs, giving detailed and accurate structural and electronic characterization. The Raman experiment is simple, can be done at room temperature and ambient pressure, and is quick, non-destructive and non-invasive.

Acknowledgments

The authors acknowledge Professor A Righi for providing the MWNT spectrum and Dr A C Ferrari for valuable discussions. This work was supported by the Instituto de Nanociências, Brazil. AJ and AGSF acknowledge financial support from CNPq (Profix) and CAPES (Prodoc)—Brazil. RS acknowledges a Grant-in-Aid (No 13440091) from the Ministry of Education, Japan. GD and MSD acknowledge support under NSF Grants DMR 01-16042, and INT 00-00408.

References

[1] Dresselhaus M S, Dresselhaus G and Avouris Ph 2001 *Carbon Nanotubes: Synthesis, Structure, Properties and Applications* (*Springer Series in Topics in Applied Physics* vol 80) (Berlin: Springer)
[2] Hafner J H, Cheung C L, Oosterkamp T H and Lieber C M 2001 *J. Phys. Chem.* B **105** 743
[3] Jorio A, Saito R, Hafner J H, Lieber C M, Hunter M, McClure T, Dresselhaus G and Dresselhaus M S 2001 *Phys. Rev. Lett.* **86** 1118
[4] O'Connell M J *et al* 2002 *Science* **297** 593
[5] Berber S, Kwon Y-K and Tománek D 2000 *Phys. Rev. Lett.* **84** 4613
[6] Thomsen C and Reich S 2000 *Phys. Rev. Lett.* **85** 5214
[7] Saito R, Jorio A, Souza Filho A G, Dresselhaus G, Dresselhaus M S and Pimenta M A 2002 *Phys. Rev. Lett.* **88** 027401
[8] Martin R M and Falicov L M 1983 *Light Scattering in Solids I* (*Springer Series in Topics in Applied Physics* vol 8) ed M Cardona (Berlin: Springer) chapter 3, p 70
[9] Dresselhaus M S and Eklund P C 2000 *Adv. Phys.* **49** 705
[10] Lin M F 2000 *Phys. Rev.* B **62** 13153
[11] Bozović I, Bozović N and Damnjanović M 2000 *Phys. Rev.* B **62** 6971
[12] Grüneis A, Saito R, Samsonidze Ge G, Kimura T, Pimenta M A, Jorio A, Souza Filho A G, Dresselhaus G and Dresselhaus M S 2003 *Phys. Rev.* B **67** 165402
[13] Reich S, Maultzsch J, Thomsen C and Ordejón P 2002 *Phys. Rev.* B **66** 035412
[14] Saito R, Dresselhaus G and Dresselhaus M S 1998 *Physical Properties of Carbon Nanotubes* (London: Imperial College Press)
[15] Kataura H, Kumazawa Y, Maniwa Y, Uemezu I, Suzuki S, Ohtsuka Y and Achiba Y 1999 *Synth. Met.* **103** 2555
[16] Milnera M, Kürti J, Hulman M and Kuzmany H 2000 *Phys. Rev. Lett.* **84** 1324
[17] Souza Filho A G *et al* 2003 unpublished
[18] Kürti J, Zólyomi V, Kertesz M, Sun G, Baughman R H and Kuzmany H 2003 unpublished
[19] Jorio A *et al* 2002 *Phys. Rev.* B **66** 115411
[20] Jorio A *et al* 2001 *Phys. Rev.* B **63** 245416
[21] Souza Filho A G, Jorio A, Hafner J H, Lieber C M, Saito R, Pimenta M A, Dresselhaus G and Dresselhaus M S 2001 *Phys. Rev.* B **63** 241404R
[22] Pimenta M A, Marucci A, Empedocles S, Bawendi M, Hanlon E B, Rao A M, Eklund P C, Smalley R E, Dresselhaus G and Dresselhaus M S 1998 *Phys. Rev.* B **58** R16016
[23] Brown S D M, Jorio A, Corio P, Dresselhaus M S, Dresselhaus G, Saito R and Kneipp K 2001 *Phys. Rev.* B **63** 155414
[24] Jiang C, Kempa K, Zhao J, Schlecht U, Kolb U, Basché T, Burghard M and Mews A 2002 *Phys. Rev.* B **66** 161404
[25] Dresselhaus M S and Dresselhaus G 1981 *Adv. Phys.* **30** 139
see also Dresselhaus M S and Dresselhaus G 2002 *Adv. Phys.* **50** 1–186
[26] Rao A M *et al* 1997 *Science* **388** 257
[27] Jorio A *et al* 2002 *Phys. Rev.* B **65** 155412
[28] Jorio A *et al* 2003 *Phys. Rev. Lett.* **90** 107403
[29] Kasuya A, Sasaki Y, Saito I, Tohji K and Nishina Y 1997 *Phys. Rev. Lett.* **78** 4434
[30] Maultzsch J, Reich S and Thomsen C 2002 *Phys. Rev.* B **65** 233402
[31] Maultzsch J, Reich S, Schlecht U and Thomsen C 2003 *Phys. Rev. Lett.* **91** 087402
[32] Souza M, Fantini C, Pimenta M A and Jorio A 2003 unpublished
[33] Jorio A, Dresselhaus G, Dresselhaus M S, Souza M, Dantas M S S, Pimenta M A, Rao A M, Saito R, Liu C and Cheng H M 2000 *Phys. Rev. Lett.* **85** 2617
[34] Dobardzić E, Milosević I, Nikolić B, Vuković T and Damnjanović M 2003 *Phys. Rev.* B **68** 045408
[35] Ajiki H and Ando T 1994 *Physica* B **201** 349

[36] Marinopoulos A G, Reining L, Rubio A and Vast N 2003 *Phys. Rev. Lett.* **91** 046402
[37] Duesberg G S, Loa I, Burghard M, Syassen K and Roth S 2000 *Phys. Rev. Lett.* **85** 5436
[38] Gommans H H, Alldredge J W, Tashiro H, Park J, Magnuson J and Rinzler A G 2000 *J. Appl. Phys.* **88** 2509
[39] Jorio A *et al* 2002 *Phys. Rev.* B **65** R121402 (Rapid communication)
[40] Tang Z K, Wang N, Zhang X X, Wang J N, Chan C T and Sheng P 2003 *New J. Phys.* at press
[41] Ferrari A C and Robertson J 2000 *Phys. Rev.* B **61** 14095
[42] Souza Filho A G, Jorio A, Samsonidze Ge G, Dresselhaus G, Pimenta M A, Dresselhaus M S, Swan A K, Ünlü M S, Goldberg B B and Saito R 2003 *Phys. Rev.* B **67** 035427
[43] Brar V W, Samsonidze Ge G, Dresselhaus G, Dresselhaus M S, Saito R, Swan A K, Ünlü M S, Goldberg B B, Souza Filho A G and Jorio A 2002 *Phys. Rev.* B **66** 155418
[44] Samsonidze Ge G, Saito R, Jorio A, Souza Filho A G, Grüneis A, Pimenta M A, Dresselhaus G and Dresselhaus M S 2003 *Phys. Rev. Lett.* **90** 027403
[45] Zólyomi V, Kürti J, Grüneis A and Kuzmany H 2003 *Phys. Rev. Lett.* **90** 157401
[46] Kneipp K *et al* 2000 *Phys. Rev. Lett.* **84** 3470
[47] Corio P, Brown S D M, Marucci A, Pimenta M A, Kneipp K, Dresselhaus G and Dresselhaus M S 2000 *Phys. Rev.* B **61** 13202
[48] Kneipp K, Jorio A, Kneipp H, Brown S D M, Shafer K, Motz J, Saito R, Dresselhaus G and Dresselhaus M S 2001 *Phys. Rev.* B **63** 081401
[49] Lefrant S, Baltog I, Baibarac M, Schreiber J and Chauvet O 2002 *Phys. Rev.* B **65** 235401
[50] Kuhlmann U, Jantoljak H, Pfänder N, Bernier P, Journet C and Thomsen C 1998 *Chem. Phys. Lett.* **294** 237
[51] Ugawa A, Rinzler A G and Tanner D B 1999 *Phys. Rev.* B **60** R11305
[52] Niyogi S, Hamming M A, Hu H, Zhao B, Bhowmik R S P and Itkis M E 2002 *Acc. Chem. Res.* **35** 1105
[53] Strano M S, Miller M K, Allen M J, Moore V C, O'Connell M J, Kittrell C, Hauge R H and Smalley R E 2003 *J. Nanosci. Nanotechnol.* at press
[54] Benoit J M, Buisson J P, Chauvet O, Godon C and Lefrant S 2002 *Phys. Rev.* B **66** 073417
[55] Zhao X, Ando Y, Qin L-C, Kataura H, Maniwa Y and Saito R 2002 *Appl. Phys. Lett.* **81** 2550
[56] Leite C F 2001 Investigação Micro-Raman de Nanotubos de Carbono Alinhados *PhD Thesis* Universidade Federal de Minas Gerais, Belo Horizonte, MG, Brazil
[57] Corio P, Santos P S, Pimenta M A and Dresselhaus M S 2002 *Chem. Phys. Lett.* **360** 557